Nuclear Engineering and Design 265 (2013) 772–784

Contents lists available at ScienceDirect

Nuclear Engineering and Design

journal homepage: www.elsevier.com/locate/nucengdes

Benchmarking LWR codes capability to model radionuclide deposition within SFR containments: An analysis of the Na ABCOVE tests

Luis E. Herranz[a,1], Monica Garcia[a,*], Sonia Morandi[b,2]

[a] CIEMAT, Unit of Nuclear Safety Research, Av. Complutense, 40, 28040 Madrid, Spain
[b] Nuclear and Industrial Plant Safety Team, Power Generation System Department, RSE, via Rubattino 54, 20134 Milano, Italy

HIGHLIGHTS

- Assessment of LWR codes capability to model aerosol deposition within SFR containments.
- Original hypotheses proposed to partially accommodate drawbacks from Na oxidation reactions.
- A defined methodology to derive a more accurate characterization of Na-based particles.
- Key missing models in LWR codes for SFR applications are identified.

ARTICLE INFO

Article history:
Received 12 October 2012
Received in revised form 20 May 2013
Accepted 23 May 2013

ABSTRACT

Postulated BDBAs in SFRs might result in contaminated-coolant discharge at high temperature into the containment. A full scope safety analysis of this reactor type requires computation tools properly validated in all the related fields. Radionuclide transport, particularly within the containment, is one of those fields. This sets two major challenges: to have reliable codes available and to build up a sound data base. Development of SFR source term codes was abandoned in the 80's and few data are available at present. The ABCOVE experimental programme conducted in the 80's is still a reference in the field.

Postulated BDBAs in SFRs might result in contaminated-coolant discharge at high temperature into the containment. A full scope safety analysis of this reactor type requires computation tools properly validated in all the related fields. Radionuclide deposition, particularly within the containment, is one of those fields. This sets two major challenges: to have reliable codes available and to build up a sound data base. Development of SFR source term codes was abandoned in the 80's and few data are available at present. The ABCOVE experimental programme conducted in the 80's is still a reference in the field.

The present paper is aimed at assessing the current capability of LWR codes to model aerosol deposition within a SFR containment under BDBA conditions. Through a systematic application of the ASTEC, ECART and MELCOR codes to relevant ABCOVE tests, insights have been gained into drawbacks and capabilities of these computation tools. Hypotheses and approximations have been adopted so that differences in boundary conditions between LWR and SFR containments under BDBA can be accommodated to some extent.

Two major outcomes result from this study: a reasonable approximation to the BDBA SFR scenario can be achieved with LWR codes if suitable hypotheses are made and development and implementation of new models is mandatory to enhance predictability to the required level in safety analyses. Vaporization, nucleation and oxidation of Na and turbulent agglomeration of particles are phenomena, for which models should be developed and implemented. Additionally, the importance of a good morphological characterization of aerosol particles has been highlighted.

1. Introduction

Characterization and behaviour of in-containment nuclear aerosols and fission products in case of a severe accident is a matter of fundamental importance for assessing the radiological consequences and for setting up suitable filtering systems and even reactor components.

* Corresponding author. Tel.: +34 913466577; fax: +34 913466233.
E-mail addresses: luisen.herranz@ciemat.es (L.E. Herranz), monica.gmartin@ciemat.es (M. Garcia), sonia.morandi@rse-web.it (S. Morandi).
[1] Tel.: +34 913466219; fax: +34 913466233.
[2] Tel.: +39 023992563; fax: +39 023995626.

0029-5493/$ – see front matter © 2013 Elsevier B.V. All rights reserved.
http://dx.doi.org/10.1016/j.nucengdes.2013.05.030

Nomenclature

Kn	Knudsen number
$C_{fireball}$	heat capacity of Fire-Ball (J/K)
C_m	Cunningham slip correction factor
c_p	specific heat capacity (J/kg K)
$c_p(Na_{aero})$	specific heat capacity of sodium (J/kg K)
c_t	thermal accommodation coefficient
D	equivalent diameter of the structure (m)
d_p	particle diameter (m)
F_{slip}	slip factor
g	acceleration of gravity (m/s^2)
k_{air}	thermal conductivity of air (W/m K)
k_{gas}/k_p	ratio of thermal conductivity of gas over that for aerosol particle
M_s	molecular weight of water (kg/mol)
$m(Na_{aero})$	mass of sodium aerosols (kg)
Nu	Nusselt number
q''	heat flux (W/m^2)
Ra	Rayleigh number
$S_{fireball}$	Fire-Ball surface (m^2)
STICK	particle sticking coefficient
T_g	gas temperature (K)
T_w	wall temperature (K)
T_{max}	maximum temperature (K)
t	time (s)
v_{diff}	diffusive deposition velocity (m/s)
v_{dph}	diffusiophoretic deposition velocity (m/s)
v_{grav}	gravitational deposition velocity (m/s)
v_{therm}	thermophoretic deposition velocity (m/s)
W_{cond}	condensation mass flux to the surface (kg/s m^2)
X_s	mole fraction of water vapour in the bulk gas
Y	weighting factor
X_{NC}	mole fraction of noncondensible gases in the bulk gas

Greek symbols

ΔT	temperature difference between the atmosphere and the wall (K/m)
ΔT_r^{max}	relative deviation of the maximum temperature
∇T	temperature gradient at the structure surface (K/m)
Δt	time difference (s)
α	numerical factor
γ	agglomeration shape factor
δ_{diff}	diffusion boundary layer thickness (m)
δ_{therm}	boundary layer thickness (m)
ε	turbulence energy dissipation rate (m^2/s^3)
ε_r	relative error
μ	viscosity (N s/m^2)
ρ_{gas}	gas density (kg/m^3)
$\rho(Na_{aero})$	density of sodium aerosols (kg/m^3)
ρ_p	particle density (kg/m^3)
ρ_s	saturation density of water vapour (kg/m^3)
σ	Boltzmann constant (J/s m^2 K^4)
χ	aerodynamic shape factor

Search for an enhanced sustainability of future Sodium-cooled Fast Reactors (SFR), has launched investigations to optimize several aspects of their safety. Postulated Beyond Design Basis Accidents (BDBAs) in SFRs might result in contaminated-coolant discharge at high temperature into the containment. As a consequence of the high chemical reactivity of sodium (Na) with air and steam, it would undergo oxidation within the containment atmosphere. The exothermic nature of the chemical reactions taking place and the high level of turbulence in the reaction area, would determine to a good extent particle size, population and radionuclide partitioning among particles and gas phase. Hence, radioactive source term to the environment would depend on in-containment Na-based aerosol behaviour. It is of utmost importance for a full scope safety analysis of SFRs, to have computation tools available and properly validated against a sound data base, particularly in the field of radionuclide deposition within the containment.

Much of the analytical capability developed for source term analysis of SFRs was developed by mid 1980-ies. At that time, the main drawbacks of the analytical tools were stated to be (Dunbar and Fermandjian, 1984; Dunbar, 1985; Fermandjian, 1985): particle characterization and particle–particle interaction processes. Since then nuclear aerosol community focused mostly on the study of aerosol transport in Light Water Reactors (LWRs) (Allelein et al., 2009; Herranz et al., 2010). At present, most of those analytical capabilities have been lost. This fact, together with the similarities between LWR and SFR source term (Herranz et al., 2012), suggested to check the Source Term LWR codes capability to deal with in-containment SFR scenarios in case of a BDBA. Nonetheless, existing LWR integral codes would need to be furnished with some specific models related to SFR aerosol generation and fission product partitioning as a *sine-qua-non* condition to get a proper characterization of particles and airborne fission product inventory.

The present paper is aimed at assessing the current capability of LWR codes to model aerosol deposition within a SFR containment under BDBA conditions. Through a systematic application of the ASTEC, ECART and MELCOR codes to relevant ABCOVE tests, insights have been gained into drawbacks and capabilities of these computation tools. Hypotheses and approximations have been adopted so that differences in boundary conditions between LWR and SFR containments under BDBA can be properly accommodated.

This work is framed under the Collaborative Project on European Sodium Fast Reactor (CP-ESFR – 2009–2012) project that was launched within the 7th EC Framework Programme (Fiorini, 2009), as part of the Generation IV initiative (http://www.gen-4.org).

2. Benchmark – boundary conditions

This paper is focused on the current LWR modelling capabilities to address in-containment aerosol deposition under SFR accident conditions. With this aim, the ASTEC, ECART and MELCOR codes responses to the Aerosol Behaviour Code Validation and Evaluation (ABCOVE) tests scenarios have been analysed and discussed (Klein-Hessling and Schwinges, 1998; Parozzi et al., 2011; Gauntt et al., 2005). The benchmark scope is limited to the ABCOVE tests because they were the only ones reported in enough detail as to allow setting reliable and meaningful data-predictions comparisons.

2.1. Codes description

The three analytical tools used are fully integrated, engineering-level computer codes that model the progression of severe accidents in LWRs. In particular, aerosol modelling in all of them is based on the MAEROS code (Gelbard, 1982), a multisection, multicomponent aerosol dynamics code that evaluates the size distribution of each type of aerosol mass (bins) as a function of time.

However, some differences found in the way each code approximates specific parameters and/or variables involved in the deposition mechanisms equations might well cause discrepancies on the final mass distribution which magnitude would depend on the scenario modelled. A good example of potential relevance in the SFR containment under a postulated accident is the thermophoretic deposition velocity (Table 1).

Table 1
Formulation for the deposition mechanisms.

Deposition phenomena	ASTEC	MELCOR	ECART
Gravitational	$v_{grav} = d_p^2 \cdot \rho_p \cdot g \cdot C_m / 18 \cdot \mu \cdot \chi$		
Diffusion	$v_{diff} = \sigma T_g C_m / 3\pi\mu\chi\, d_p\, \delta_{diff}$		
	δ_{diff} 10^{-3} m	δ_{diff} 10^{-5} m	δ_{diff} 10^{-4} m
Thermophoresis	$v_{therm} = \left(3\mu\ C_m (c_t\,\mathrm{Kn} + k_{gas}/k_p)/2\chi\rho_{gas}\ T_w(1+3F_{slip}\,\mathrm{Kn})(1+2c_t\,\mathrm{Kn}+k_{gas}/k_p)\right)\cdot\nabla T$		
	$\nabla T = \Delta T/\delta_{therm}$	$\nabla T = -q''/k_{air}$	$\nabla T = \Delta T/\delta_{therm}$
	ΔT temperature difference between the atmosphere and the wall	q'' heat flux	ΔT temperature difference between the atmosphere and the wall
	δ_{therm} 10^{-3} m	k_{air} thermal conductivity of air	$\delta_{therm} = D/\mathrm{Nu}$
Diffusiophoresis	$v_{dph} = \left(\sqrt{M_s}/X_s\sqrt{M_s} + X_{NC}\sqrt{M_s}\right)\left(W_{cond}/\rho_{gas}\right)$ if $W_{cond} \geq 0$ (condensation)		
	$v_{dph} = W_{cond}/\rho_s$ if $W_{cond} < 0$ (evaporation)		ECART takes into account the diffusiophoresis phenomena only for condensation

Another source of discrepancies might be all related processes governing the boundary conditions of Table 1 equations, like the temperature. A review of the turbulent natural convection correlations (one of the heat transfer mode anticipated within SFR containments), has revealed noticeable differences (20–25%) in the predictions of Nusselt (Nu) as Rayleigh (Ra) is over 10^{10} (Fig. 1). In addition, differences might also come from the gas properties estimates, although these have been proved not to be significant.

2.2. Experimental scenarios

The ABCOVE experiments were conducted in the Containment System Test Facility (CSTF) vessel at the HEDL (Handford Engineering Development Laboratory, USA). The containment is a cylindrical steel vessel (7.6 m diameter, 20.3 m high) of about 852 m^3 (Fig. 2). The vessel is furnished with instrumentation to monitor both thermal–hydraulics and aerosol behaviour. In particular, the atmosphere oxygen content, gas temperature, aerosol concentration and size and final aerosol mass distribution, were recorded. A more thorough description of experimental aspects may be found in Hilliard et al. (1985) and Souto et al. (1994).

Three experiments of the ABCOVE program have been chosen: AB5, AB6 and AB7. These three tests can be grouped according to the sodium fire type. In the AB5 and AB6 tests, a Na spray fire was the origin of aerosols; in the AB7 test, though, the main aerosols source was a small pool fire. Besides, in the AB6 and AB7 tests, NaI aerosols were injected as representative of fission product bearing particles. A noticeable difference between these two tests, however, was the timing of NaI injection with respect to the Na fire; whereas in AB6 NaI injection overlapped with the sodium spray fire, in AB7, NaI got into the vessel after the Na pool fire had ended. The test conditions are summarized in Table 2.

Table 2
Summary of test conditions.

Initial containment atm.	AB5	AB6	AB7
T (mean) (K)	302.25	304.15	297.05
Pressure (MPa)	0.122	0.114	0.118
Dew point (K)	289.15 ± 2	285.35	274.65
Na spray/spill (AB7)			
Na spray/spill rate (g/s)	256 ± 15	42.8 ± 2.1	322
Spray/pool periods duration (s)	13–885	620–5400	20–600
Na sprayed/delivered (kg)	223 ± 11	204.7 ± 4.1	6.434
Na initial T (K)	836.15	833.15	863.15
NaI source			
Release rate (g/s)	–	0.14	0.197
Spray period (s)	–	0–3000	600–2400
NaI released (g)	–	420	354.6

In the AB5 test (1982), a single-species aerosol was generated by spraying sodium at high flow rate into the air atmosphere. The injection took place through two facing upward nozzles located at

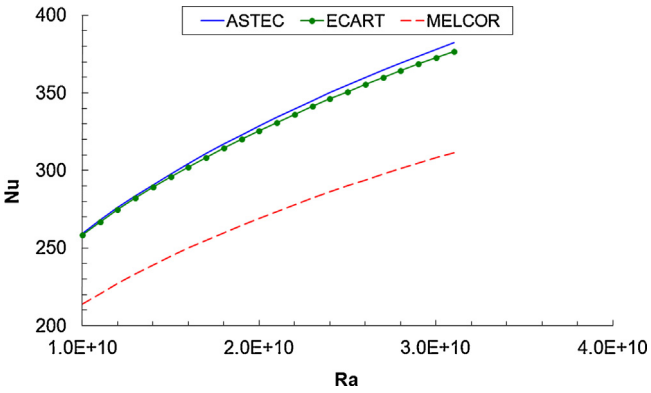

Fig. 1. Nusselt number vs. Rayleigh number.

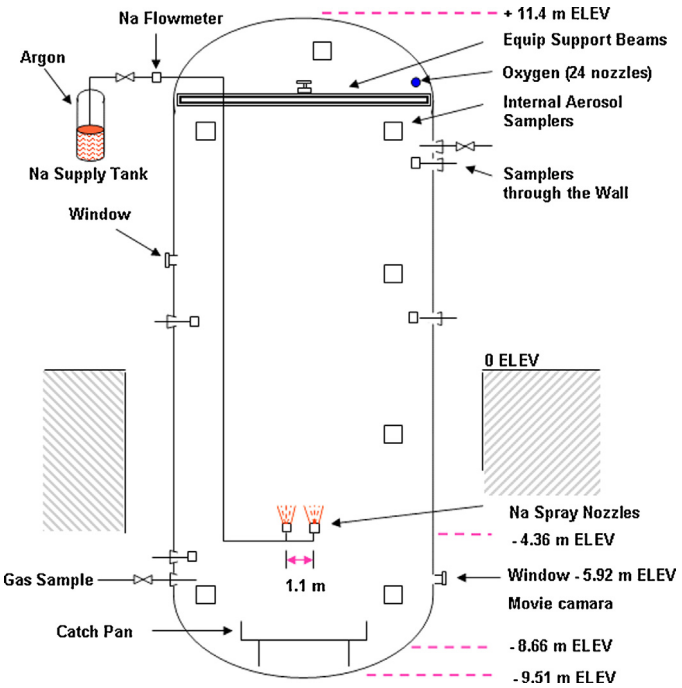

Fig. 2. CSTF vessel arrangement for test AB5.

5.15 m from the vessel lower head. A total of 223 kg of sodium was sprayed over 872 s. The primary objective of the AB5 was to provide experimental data on Na aerosols during a sodium spray fire.

The test AB6 (1983) simulated an accident in which fission product iodine reached containment in the form of NaI particles while a sodium spray fire was occurring. The amount of combustion particles was roughly 500 times higher (in mass) than the NaI and it lasted longer. The NaI was injected 620 s before the Na aerosols and lasted nearly 3000 s. A total of 205 kg of Na was injected during 4780 s through a single spray nozzle located at 5 m from the vessel lower head. The focus of the test was to investigate the capability of combustion aerosols to washout the NaI particles by co-agglomeration and subsequent deposition.

During the AB7 test (1984), NaI was released into the containment vessel atmosphere after the end of a small sodium pool fire. The primary purpose of test AB7 was to demonstrate the co-agglomeration of the two aerosol species under mild thermal conditions (i.e., no thermal decomposition is expected). The AB7 test began with the injection of sodium into the containment vessel. The sodium spraying line failed immediately after the initiation of the sodium flow. The failure was such that sodium leaked from the line and fell to the personnel deck at 7.6 m from the vessel bottom, where it formed a pool and burned as a pool fire (a total of 6.434 kg of Na was delivered). The flow of sodium was stopped 20 s later. The duration of the pool fire is believed to have been approximately 10 min. The NaI aerosols injection was started at 600 s and it was kept constant until 2400 s.

2.3. Major hypotheses and approximations

One of the specific features of accident containment scenarios in SFRs is the sodium (Na) oxidation with surrounding air and steam. The absence of this reaction in LWR containments makes it be one of the major challenges for LWR codes when modelling SFR accident scenarios: the aerosol and energy sources resulting from Na-air/steam interactions.

2.3.1. Mass input

The Na-air reactions have been extensively studied (Cooper, 1980; Clough and Garland, 1971; Morewitz, 1979). One of the earliest works was the set of experiments conducted by Humphreys at ANL (Humphreys, 1958). In these experiments, hot Na (~673 K) was injected in an explosive way within a vessel atmosphere at normal conditions (similar to those in the ABCOVE tests). Main variables tested were Na amount, distribution, ejection force and steam content. According to his observations, when finely divided (i.e., sprays), high temperature molten Na is mixed with air, the dominant reaction is the formation of sodium peroxide (Na_2O_2). In addition, Newman (1983), Okano and Yamaguchi (2003) and Subramani and Jayanti (2008) stated that under unconfined conditions (i.e, unlimited oxygen), the sodium oxide formation dominates in the flame; however, whenever temperature is lower than around 900 °C the peroxide formation dominates. Based on this information, the formation of Na_2O_2 is considered as the dominant reaction:

$$2Na + O_2 \rightarrow Na_2O_2 \quad \Delta H = -5.2 \times 10^5\ J/mol \tag{1}$$

The presence of steam, on the other side, results in the formation of sodium hydroxide (NaOH):

$$Na + HOH + \frac{1}{2}Na_2O_2 \rightarrow 2NaOH \quad \Delta H = -3.6 \times 10^5\ J/mol \tag{2}$$

In the AB5 and AB6 the amount of steam in the air was rather low, so that to estimate the amount of injected aerosols, two major approximations have been made:

- Most Na gets converted to Na_2O_2 through Eq. (1).
- The maximum amount of NaOH is formed according to the available steam in the vessel (Eq. (2)).

As shown in Table 3 this approximation results in a Na_2O_2/NaOH distribution of 87%/13%, in AB5, and 89%/11%, in AB6. The generation rates have been assumed to be constant during the entire periods of Na injection (i.e., 0.435 kg/s and 0.0729 kg/s).

The AB7 test was carried out with a steam rich atmosphere. Given that reaction (2) is certainly fast and the presence of a steam excess, all the reacting Na has been postulated to be converted to NaOH. Unlike AB5 and AB6, based on Hilliard et al. (1985), only 27% of pooled Na has been assumed to react. As in the other tests, the generation rate has been assumed to be constant during the Na pool-fire duration (5×10^{-3} kg/s). All the specific injection information for all the tests is gathered in Table 3.

Table 3
Main aerosol characteristics.

	AB5	AB6	AB7
Na_2O_2/NaOH fraction (%)	87/13	89/11	–/100
Generation rate (kg/s)	0.435	0.0729	0.005
Total aerosol mass injected (kg)	380	350	3.3

2.3.2. Energy input

Consistently with the mass input, the energy input has been estimated based on the above Na_2O_2/NaOH distribution: 2.95×10^9 J in AB5 and 2.65×10^9 J in AB6. As assumed above, energy input rate has been defined as constant all over the injection period. In the case of AB7, the energy injected amounted to 1.34×10^7 J.

In ASTEC and MELCOR, the total amount of energy injected has been assumed to distribute evenly between the vessel atmosphere and the particles (i.e., 50%/50%). This distribution is based on the similar specific heat capacities of air and sodium particles (c_p(air) ~ 1000 J/kg K; $c_p(Na_{aero})$ ~ 1200 J/kg K). This approximation means that chemical energy distribution is a local process between Na and air surrounding Na particles and that once the energy is absorbed in-air heat transport is so effective that gas temperature becomes readily uniform. As particle-gas heat exchange is not modelled in current codes, an artificial surface representing particles has been defined. The surface area is approximated by assuming all the sodium particles collapsed in a sphere ("Fire-Ball"); the idea underneath is that most particles are created in a small region of the entire vessel volume, so that particle density is very high. Such a high density would cause a sort of heat transfer shielding for all particles inside the ball; in other words, no convection and radiation would be effective within the particle cloud. Hence, heat transfer to atmosphere and vessel walls would occur just from those particles located at the outer layer. This approach has been named "Fire-Ball" Approximation (FBA).

In order to bring FBA as close as possible to reality, the thermal capacity of sodium aerosols has been kept. By adopting the actual value of the specific heat of Na_2O_2 and NaOH, a fictitious density was estimated based on a 10^{-3} m thickness (this small value prevents any internal thermal process from being significant). The characteristics of this surface are given in Table 4. The

Table 4
Characteristic variables of the FBA (ASTEC and MELCOR codes).

	AB5	AB6	AB7
Surface area (m^2)	1.3	1.3	0.061
Thickness (m)	0.001	0.001	0.001
Density (kg/m^3)	2.9×10^5	2.7×10^5	4.9×10^4
c_p (J/kg K)	1188.72	1181.84	1488.0

Table 5
Energy input surface structure (ECART).

	AB5	AB6	AB7
Surface area (m^2) (radiative heat transfer)	270	48	8
Surface area (m^2) (convective heat transfer)	210	37	5

main hypothesis for this approximation can be written as follows:

$$S_{\text{fireball}} \cong \left(\alpha \cdot \frac{m(\text{Na}_{\text{aero}})}{\rho(\text{Na}_{\text{aero}})}\right)^{2/3} \quad (3)$$

$$C_{\text{fireball}} \approx \sum m(\text{Na}_{\text{aero}}) \cdot c_p(\text{Na}_{\text{aero}}) \quad (4)$$

$$c_p(\text{Na}_{\text{aero}}) \approx c_p(\text{air}) \quad (5)$$

A weakness of this approximation is that surface area remains constant all over time. Actually, particles remain airborne for some time and gradually get removed from atmosphere by deposition mechanisms. Therefore, this approximation should result in an overestimate of gas and vessel wall temperatures during the aerosol deposition phase.

A set of parametric cases proved that FBA meant an enhancement with respect to other approximations found in the literature (Souto et al., 1994). These results are gathered in Appendix A.

ECART modelling of heat input to the atmosphere is simpler. The code models energy injection through defining a heat structure. It is characterized by two different surface areas according to the significance of the transfer processes, so that radiative one is larger than convective one (this makes the model consistent with the conclusions of Yamaguchi and Tajima, 2006). Table 5 shows the best choice for the ABCOVE tests.

2.3.3. Nodalization and heat structures

The CSTF vessel has been modelled as a single cell (852 m^3). Five heat structures representing the top and bottom heads, the cylindrical walls and the internal components for aerosol plating and settling, have been considered (Table 6). In all heat structures, the material facing the vessel atmosphere is stainless steel. As in the experiment, the vessel walls have been modelled as externally insulated with fibreglass.

To model the thermal–hydraulic variables, the CSTF vessel atmosphere and the contacting surfaces are initially set to room conditions. Natural convection heat transfer has been activated. Radiation heat transfer has been modelled through a gray gas approximation, assuming a value of 0.40 for the Na emissivity (Lee and Choi, 1997) in MELCOR and ASTEC simulations while for ECART simulation, 0.25 is set for the Na emissivity (Yamaguchi and Tajima, 2006).

2.3.4. Aerosol modelling

The main input specified variable characterizing particles is their size. The Mass Median Diameter (MMD) and Geometric Standard Deviation (GSD) used (Table 7), have been taken from measurements (Souto et al., 1994). A lognormal distribution for all the tests has been assumed. It is worth noting that particles were assumed to be non-hygroscopic (relative humidity was very low in all the tests and it was assumed to instantaneously react with Na).

In addition, a set of aerosol coefficients characterizing particle form, conductivity and process lengths, etc. are user options. A methodology to define the best set of particle parameters was developed and it is presented in detail in the Appendix B. In the base case scenario, the code's default values have been assumed.

Table 6
Surface areas of heat structures.

Heat structures surface (m^2)	
Top head	63.0
Cylinder walls	395.0
IC for plating	232.0
Bottom head	45.604
IC for settling	42.696

Table 7
Values for aerosol characterization.

	AB5	AB6	AB7
MMD (μm)	0.50	0.50	0.54
GSD	1.5	2.0	2.0

3. Results and analysis

In this section, code predictions and data are compared as an assessment of the code predictability. However, it should be indicated that data points were taken from old reports in the open literature and some of the figures shown there were presented in log plots. This means that our data points are automatically affected by some artificial uncertainty associated to the withdrawal process.

3.1. Thermal–hydraulics

In order to assess thermal–hydraulics, comparisons are set in terms of temperature. In this lumped analysis an 852 m^3 vessel is represented by a single node. In other words, modelling assumes that the whole vessel atmosphere is uniform virtually; this might not be the case for a so large vessel with a limited region of intense energy input (Na injection), unless working heat transfer mechanisms and the resulting circulation patterns had been capable of making the vessel atmosphere uniform. Therefore, only reasonable matching can be expected between data and code estimates.

According to data (Figs. 3–5), gas temperature evolution may be described in four phases:

- Fast heat-up (phase I); a direct consequence of energy from the exothermal Na reactions absorbed by the vessel gas before any heat transfer mechanism becomes noticeably effective.
- Heat-up slowdown (phase II); energy is still captured by the vessel atmosphere but temperature difference between gas bulk and vessel walls makes natural convection significant and, as a result, a significant fraction of the energy input gets removed.
- Fast cooling (phase III); once Na injection ends, the energy input is also over (very fast kinetics of oxidation) and, as a consequence, the gas phase moves fast to set a new thermal level with no heat source.

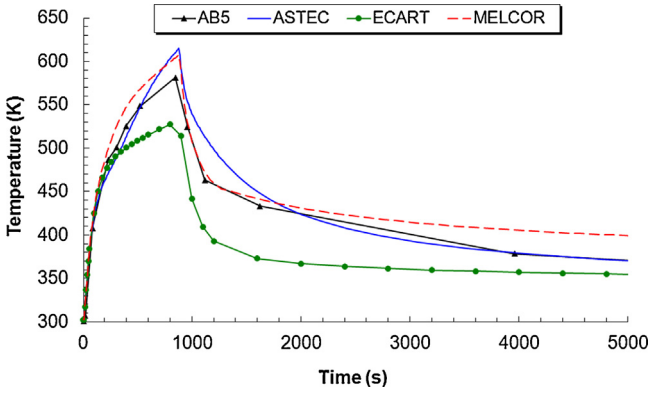

Fig. 3. Atmosphere temperature – AB5.

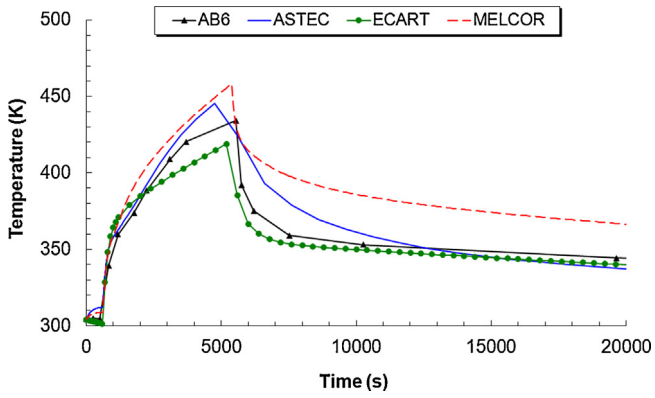

Fig. 4. Atmosphere temperature – AB6.

- Smooth cooling (phase IV); natural convection cooling eventually governs any temperature change in the "long term".

A couple of notes should be added to the previous paragraph. In the AB7 test, this phasing of temperature is not so evident because the energy source was much smaller in this experiment. The term "long term" in this section means after Na injection is over. In other words, the first two phases would be "short term", whereas the two last ones would be "long term".

According to Figs. 3 and 4, codes matched data trends as long as temperature change is driven by energy injection or heat source elimination (phases I and III); in the phase I, the consistency with data is even quantitative. Major differences, though, appear during the slowdown phase, in which removal mechanisms compete with the energy input. Both in this period and in the fourth one (smooth cooling), codes behave notably different. MELCOR closely follows data in AB5; however, once energy input is over, its cooling prediction in the AB6 test looks insufficient. ASTEC responds analogously while energy is coming into the vessel, but its cooling slope in phases III and IV seems too moderate though it matches data in the end. Contrary to MELCOR and ASTEC, ECART shows in all the cases a thermal level lower than measured; in addition, it behaved differently in AB5 and AB6: whereas in AB5 deviations are noticeable, in AB6 it follows experimental trends remarkably.

In order to quantify code's deviations from data, two indicators are proposed: relative deviation of the maximum temperature (ΔT_r^{max})

$$\Delta T_r^{max} = \frac{T_{code}^{max} - T_{data}^{max}}{T_{data}^{max}} \tag{6}$$

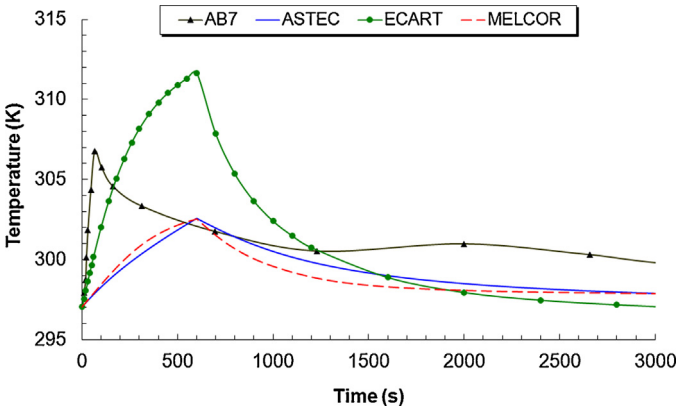

Fig. 5. Atmosphere temperature – AB7.

Table 8
Codes accuracy.

		AB5	AB6	AB7
ASTEC	ΔT_r	0.058	0.025	−0.016
	$dT/dt\|_r$	1.88	1.87	1.85
ECART	ΔT_r	−0.093	−0.035	0.016
	$dT/dt\|_r$	−0.68	0.46	7.88
MELCOR	ΔT_r	0.045	0.055	−0.016
	$dT/dt\|_r$	−0.23	1.74	0.22

and relative deviation of the temperature slope in the very long term ($dT/dt|_r$)

$$\left.\frac{dT}{dt}\right|_r = \frac{dT/dt|_{code} - dT/dt|_{data}}{dT/dt|_{data}} \quad 2t_{T\,max} \le \Delta t \le 4t_{T\,max} \tag{7}$$

The former gives a measure of the short term accuracy, whereas the latter gives an indication of the temperature evolution in the long term. Even though, both of them have been reported in Table 8 for the three tests, it is considered that the most significant is ΔT_r. On one side, during the long term temperature slope is quite small, so that $dT/dt|_r$ becomes too sensitive to slope differences. On the other, and more importantly, the major impact of thermal–hydraulics on aerosol behaviour will happen at the early stages of Na oxidation, when the large thermal gradients enhance the thermophoretic deposition of the still small particles (i.e., unagglomerated).

In sight of the ΔT_r values in the table, no major deviations are reported concerning any of the codes used, all of them look reasonable given the uncertainties affecting data, as discussed at the beginning of Section 3, and the single-cell approach adopted in the modelling.

3.2. Aerosol behaviour

3.2.1. Base case

All the modelling aspects discussed in previous sections apply to this base case (BC), which results are presented below.

Figs. 6–8 show the aerosol mass evolution in each test, as measured and as predicted by the codes. It is worth noting that in all the cases the analytical tools capture the overall trends, but they notably deviate from data in specific values as significant as the maximum airborne mass and the time maxima are reached. Just to give an example, in the test AB5, the ECART's relative error in the airborne mass peak was over 90% and it was delayed more than a factor of 1.5 with respect to the experimental time. The reason behind such discrepancies is postulated to be agglomeration.

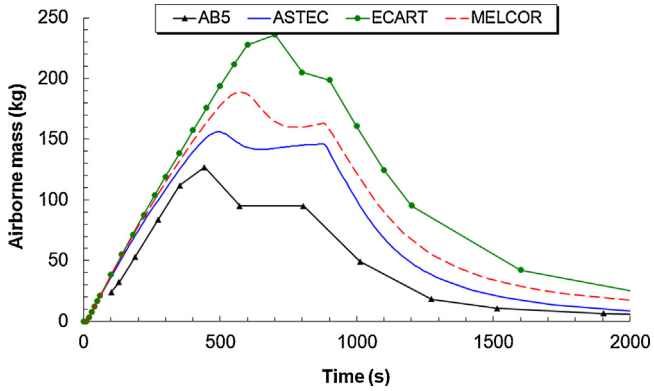

Fig. 6. Airborne mass as a function of time (BC) – AB5.

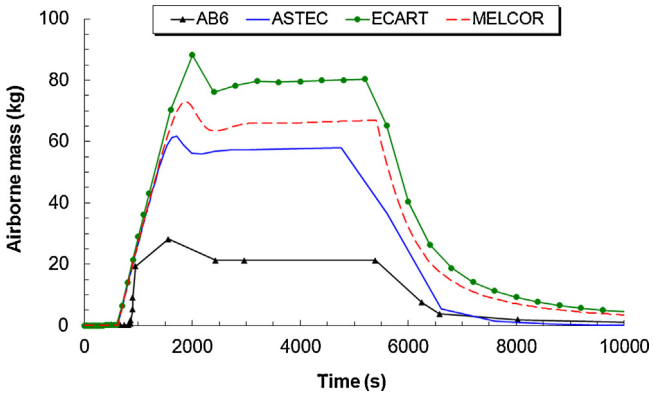

Fig. 7. Airborne mass as a function of time (BC) – AB6.

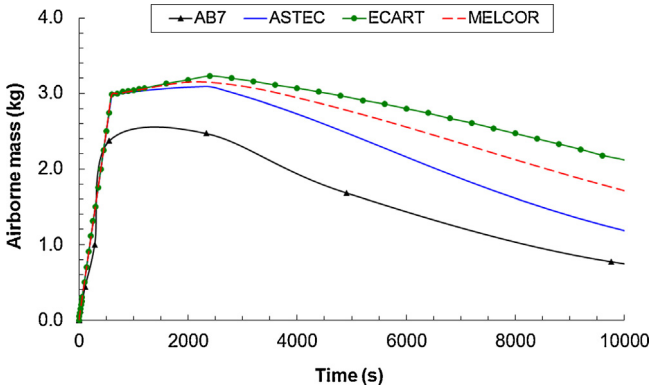

Fig. 8. Airborne mass as a function of time (BC) – AB7.

As shown in Fig. 9 for the AB5 test, experimentally, a fast particle growth was observed and it led to an early balance between injection and depletion by sedimentation. The codes, however, estimated a slower growth reaching the injection-depletion trade-off later. The notably less deviation in AB7, in which the amount of particles injected was more than 30 times smaller than in the other tests, supports this postulate.

The agglomeration rate underestimation does not necessarily mean models deficiencies. Given the large volume of the vessel and the presumably highly agitated environment over the inject point, it seems reasonable that most agglomeration had been occurred in a region smaller than the entire vessel. As agglomeration rate depends on particle concentration squared, the adopted 1-single node approach would have meant a noticeable under-estimate. Just to illustrate this discussion, if the region under the injection point

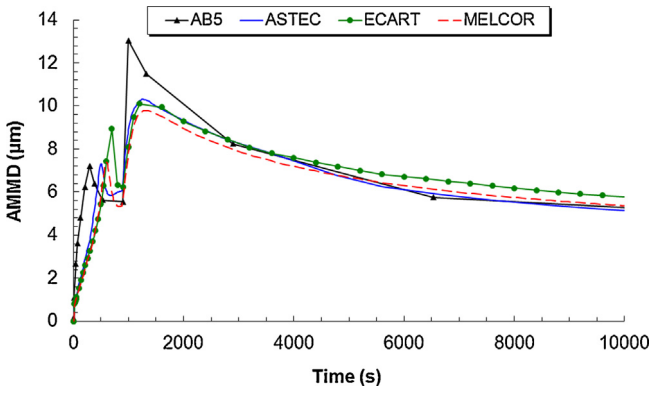

Fig. 9. AMMD as a function of time (BC) – AB5.

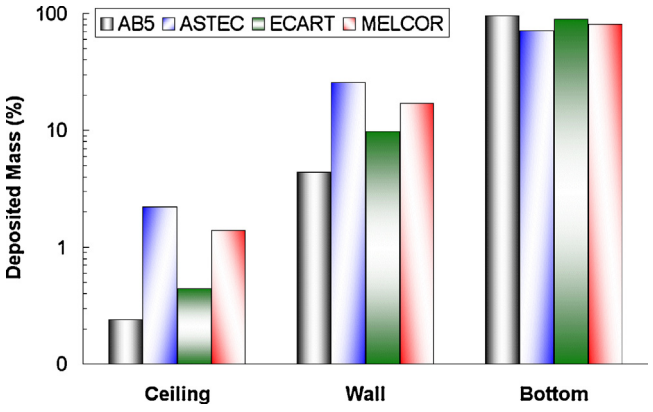

Fig. 10. Aerosol mass distribution (BC) – AB5.

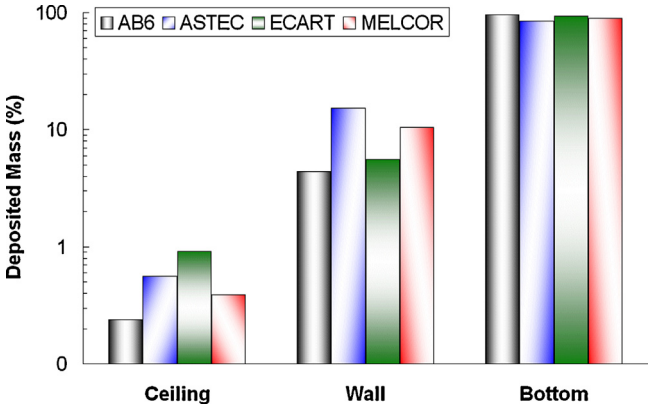

Fig. 11. Aerosol mass distribution (BC) – AB6.

(20% of the total vessel volume) would have been excluded in the agglomeration calculation, particles would have grown 1.5 times faster in the codes.

As a consequence of the deviations discussed above, the codes underpredicted the depleted mass and its distribution was different from measurements. The smaller aerosol size calculated made sedimentation less efficient than observed. This allowed other removal mechanism to play a role more significant than what it really was. This is illustrated in Figs. 10–12, where the final mass distribution in each test is shown as a fraction of the total depleted mass. Note that the ordinate axis is in logarithmic scale, which underlines the largely dominant role played by sedimentation in all the tests; this feature has been captured by the codes.

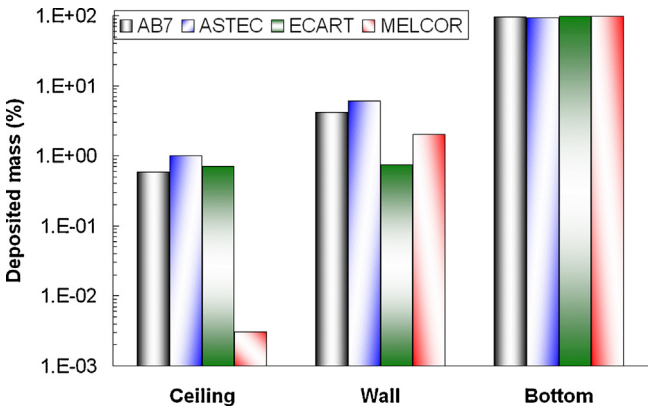

Fig. 12. Aerosol mass distribution (BC) – AB7.

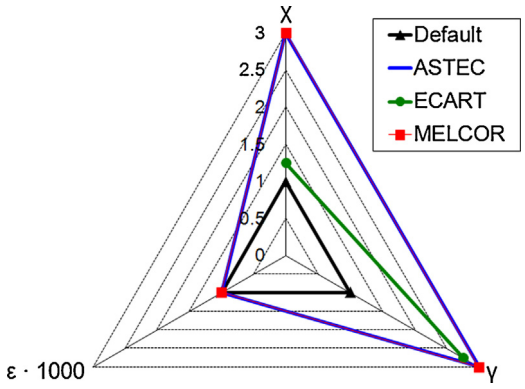

Fig. 13. Best values – AB5.

As for the differences shown among the codes, they could come from the different thermal–hydraulic boundary conditions calculated which could have had an effect on the thermophoretic mechanism. The three codes use the Talbot equation (Talbot et al., 1980) to calculate the thermophoretic deposition velocity (v_{therm}):

$$v_{\text{therm}} = \frac{3\,\mu\;C_{\text{m}}\,(c_{\text{t}}\,\text{Kn} + k_{\text{gas}}/k_{\text{p}})}{2\,\chi\,\rho_{\text{gas}}\;T_{\text{W}}\,(1+3F_{\text{slip}}\,\text{Kn})(1+2c_{\text{t}}\,\text{Kn}+k_{\text{gas}}/k_{\text{p}})}\nabla T \qquad (8)$$

Some of the variables and parameters embodied in the equation are estimated in a different way (i.e., particle slip coefficient and thermal accommodation coefficient). Analytically it has been demonstrated that under the same boundary conditions, the Talbot equation might result in differences up to a factor 1.5 between each code estimates of v_{therm}.

3.2.2. Best estimate

As said above, aerosol characterization might affect substantially the code ability to capture the experimental scenarios. To explore other possibilities than the BC one presented in Section 3.1, a methodology has been developed to reach the best possible agreement with data (Appendix B), named best estimate (BE) case. Through a three-step procedure (i.e., determination of uncertainty ranges, identification of "hard" input variables and screening out of scenarios), the best values of the particle shape factors, both dynamic and agglomeration one (χ and γ respectively), and the turbulent energy dissipation rate (ε) have been determined (ε is not imposed through the input deck in ECART). The results are shown in Figs. 13–15. It should be underlined that this methodology applies only to ASTEC and MELCOR; ECART values were found through parametric calculations. It should be noted that the largest deviations with respect to the default values were got in those tests with large particle loads (AB5 and AB6); in AB7, though, ASTEC and

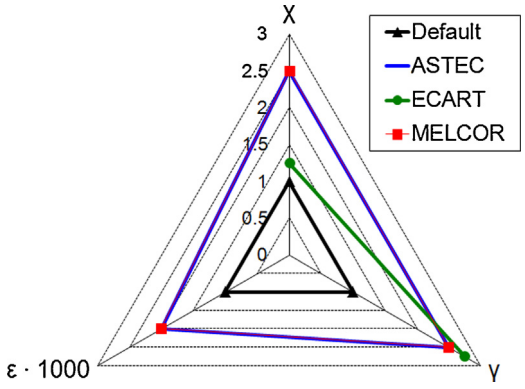

Fig. 14. Best values – AB6.

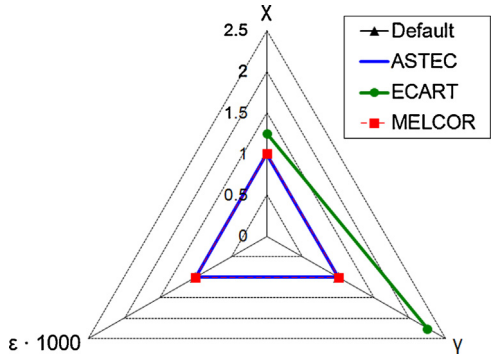

Fig. 15. Best values – AB7.

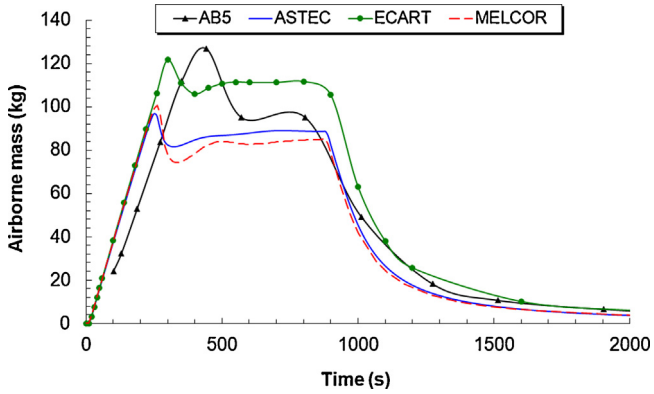

Fig. 16. Airborne mass as a function of time (BE) – AB5.

MELCOR best values coincided with the default ones. This might indicate a relation between agglomeration and particle shapes other than spherical.

The match achieved with data is shown in Figs. 16–18. As for the airborne mass, the profiles predicted looked like data's: after reaching a maximum, a moderate decrease ends up in a steady state that breaks down once injection is over. The consistency extends to the final mass distribution (Figs. 19–21), which also shows a much closer agreement to data than in the BC for all the codes. In short, all the codes capture the major results of the test in the BE case. Even ECART, which reasonably succeeded in the BC, get closer when an "aerosol BE scenario" is postulated. This improvement of the BE is even more pronounced in the case of ASTEC and MELCOR.

Finally, the "wash-out" effect of fission product simulant (NaI) by the NaO_x aerosols (mixture of Na_2O_2 and NaOH coming from sodium spray fire), is analysed in Fig. 22. The measured airborne

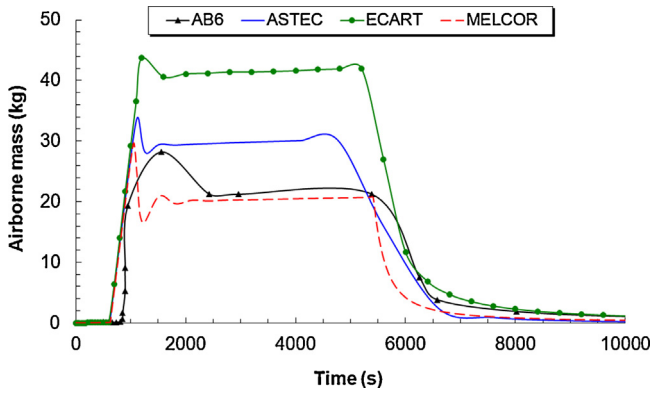

Fig. 17. Airborne mass as a function of time (BE) – AB6.

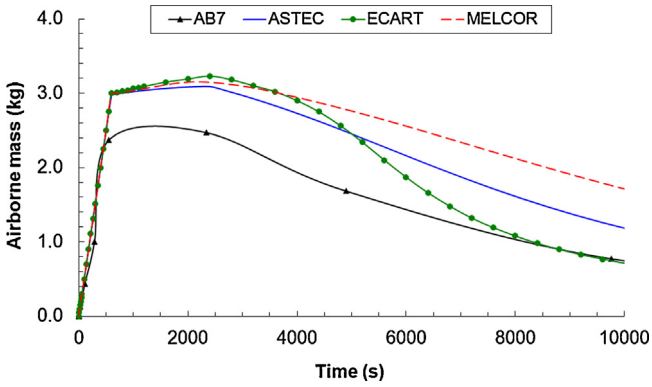

Fig. 18. Airborne mass as a function of time (BE) – AB7.

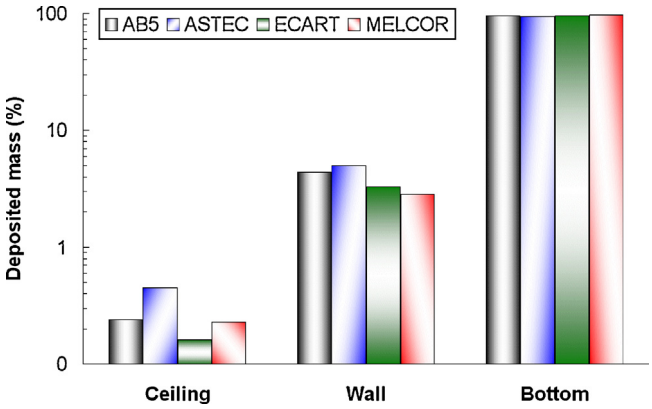

Fig. 19. Aerosol mass distribution (BE) – AB5.

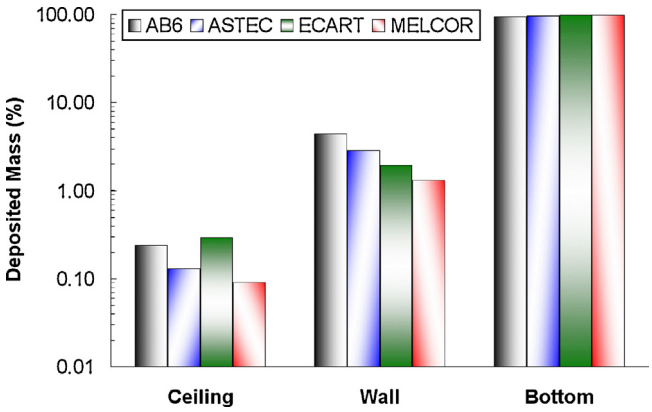

Fig. 20. Aerosol mass distribution (BE) – AB6.

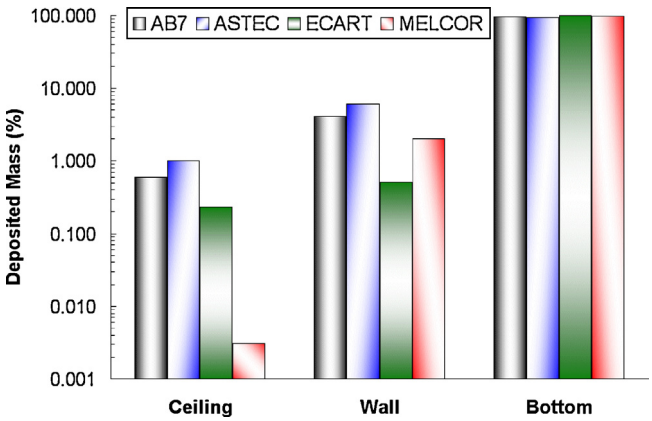

Fig. 21. Aerosol mass distribution (BE) – AB7.

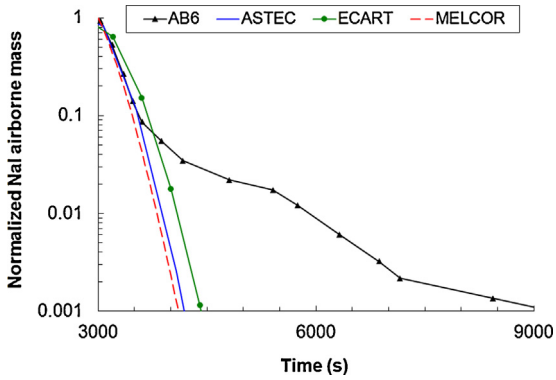

Fig. 22. NaI depletion – AB6.

NaI mass normalized with respect to the airborne mass at the end of the NaI source is shown along time; aerosol predictions are also included in their respective terms. As it can be seen, the NaI washout effect observed experimentally proceed in phases, whereas ASTEC, ECART and MELCOR did not catch that evolution, showing a too effective removal of NaI in the atmosphere.

As for the co-agglomeration of species, the AB6 simulations indicated that none of the three codes caught it. Experimentally it was shown that initially NaI co-agglomerated effectively and reduced its airborne mass rapidly; then depletion clearly slowed down as if the washout effect lost efficiency due to less NaI–NaO_x interactions and as a fraction of NaI had not agglomerated. The faster NaI experimental decay once NaO_x injection came to an end was experimentally explained as a consequence of NaI particle resuspension due to Na fires, although other explanations should be also explored, like the enhancement of any depletion mechanism due to changes in thermal–hydraulic conditions of the vessel. Contrarily to observations, all the codes matched up in their predictions: all the NaI aerosols agglomerated with the source of NaO_x.

This behaviour of the computational tools is not conservative. A potential reason might again come from the single-cell approach, which would allow co-agglomeration all over the time. However, if several cells had been set particle–particle interaction would have been estimated locally. Then, for instance, the large particles would abandon upper cells faster than smaller ones, so that the life time of particles at upper levels would have been longer than in lower cells.

4. Conclusions and further work

Three codes have been used (ASTEC, ECART and MELCOR) to model SFR accident scenarios in the containment: the ABCOVE AB5, AB6 and AB7 tests. From their response and analysis, two major conclusions might be drawn:

- Current LWR codes have the potential to be extended to the SFR domain concerning “in-containment” aerosol deposition. However, there are some areas in which additional modelling work would be needed, like the aerosol-surface heat exchange by radiation.
- Sodium based particles produced during a spray fire might be non-spherical. Whether this was confirmed, the smallest change to be made in the LWR codes would be to define other default values for parameters like shape factors. Nonetheless, the most reasonable initiative would be to launch experiments where Na-based particles could be sampled and analysed.

These conclusions, though, should be seen as preliminary since a more extensive modelling work should be pursued. This again

requests to build up a sound and reliable database on Na-based aerosols under SFR severe accidents. As noted, in the major hypotheses taken in this work, one of the most important areas requesting further experimental/theoretical work is aerosol formation/input within containment. As stated recently by Herranz et al. (2012) elsewhere, the main models to enable LWR safety codes for "in-containment" severe accident analysis would be: sodium vaporization, nucleation, radionuclides partitioning and turbulent agglomeration.

Additionally, two other outcomes resulted from this work: a set of defendable hypotheses to accommodate present drawbacks of LWR codes to model SFR severe accident scenarios, like the so called "Fire-Ball Approximation"; and a methodology that allowed identifying key aerosol input variables to focus on when modelling SFR accident scenarios and that assisted in demonstrating that under high particle concentration, Na-based particles might not be spherical. This might bridge the existing modelling gap in LWR codes for in-containment aerosol deposition until these codes become furnished, or new codes developed, with some of the models currently missing.

Acknowledgement

The authors wish to thank the partial funding received from the 7th Framework Programme of the European Commission via the CP-ESFR project (contract number 232658).

Appendix A. Fire-Ball Approximation assessment

As Na particles contact air a substantial release of thermal energy occurs at the location at which Na oxidation is taking place. Whether the specific spot is on particle surface or within the particle depends on the surface area exposed to the air available. Therefore, the energy released distributes between the particle and the surrounding gas atmosphere. As a consequence, both particle and gas temperature rise according to the energy deposited in their bulk and their specific heat. The overall picture of heat transfer at the system can be sketched as a series and parallel coupling of thermal resistance, such as shown in Fig. A.1.

In short, particles exchange thermal energy with the surrounding gas and structures; assuming that Na surface temperature is higher than those of both gas and other structures around, convection conveys thermal energy to the gas phase whereas radiation does to the structures. Additionally, the gas absorbs a fraction of the energy transferred between Na and structures.

Unlike the outlined scenario, the traditional approach used to simulate such a scenario in codes is just giving a source of thermal energy to the system atmosphere in the input deck (Souto et al., 1994). Fig. A.2 sketches this approximation and allows observing how different it is from Fig. A.1.

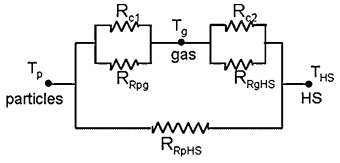

Fig. A.1. Sketched of heat transfer at the system.

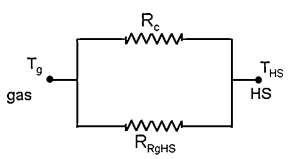

Fig. A.2. Sketched of heat transfer at the system – codes approximation.

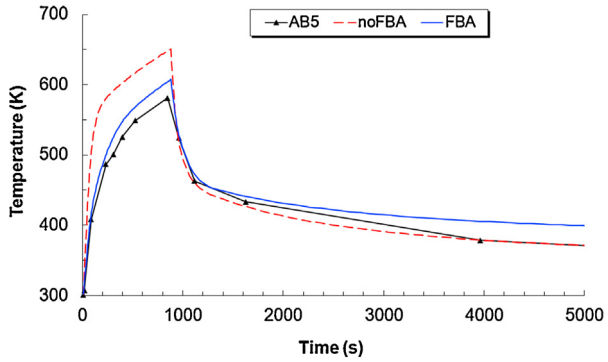

Fig. A.3. Atmosphere T – AB5 (MELCOR code).

The major limitation found in LWR codes (i.e., ASTEC, MELCOR) to capture a scenario closer to Fig. A.1 is that no radiation is foreseen between aerosol particles and heat structures around. In order to overcome the drawbacks of this classical approach, an alternative closer to reality has been proposed: the so called "Fire-Ball Approximation" (FBA).

An artificial surface representing particles is defined. The surface area is approximated by assuming all the Na particles collapsed in a sphere ("Fire-Ball"); the idea underneath is that most particles are created in a small region of the entire vessel volume, so that particle concentration results to be very high. In such a dense particle cloud a sort of heat transfer shielding between the inner particles and the outer region of the cloud happens: particles at the external layer of the cloud block any thermal radiation from inside and gas flows mainly around the cloud. As a result, no convection and radiation would be effective within the particle cloud. Hence, heat transfer to atmosphere and vessel walls would occur just from those particles located at the outer layer.

Figs. A.3 and A.4 show the in-containment atmosphere temperature with/without the FBA for AB5 and AB6 tests (noFBA/FBA). Due to the similar results found with MELCOR and ASTEC codes, only the MELCOR results have been included for the analysis. As it can be seen, the sodium spray fire predictions (AB5, AB6 tests) are in a better agreement with the experimental data during the injection period, when the impact of thermal–hydraulics on aerosol behaviour is dominant. It is worth noting that given the rough representation of an 852 m^3 vessel by just a single volume, which implicitly assumes that gas atmosphere is uniform, one should not expect better data-predictions consistency. These predictions consistency of the FBA cannot be extended to sodium pool fires. As it can be seen in Fig. A.5, the fast temperature increase and subsequent decay is not well captured using the FBA. This could arise due to the uncertainties in the test conditions associated with the

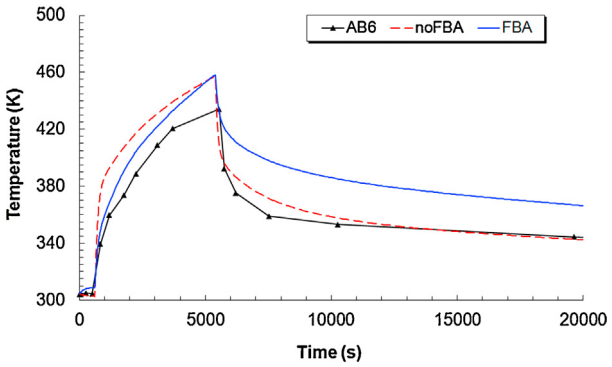

Fig. A.4. Atmosphere T – AB6 (MELCOR code).

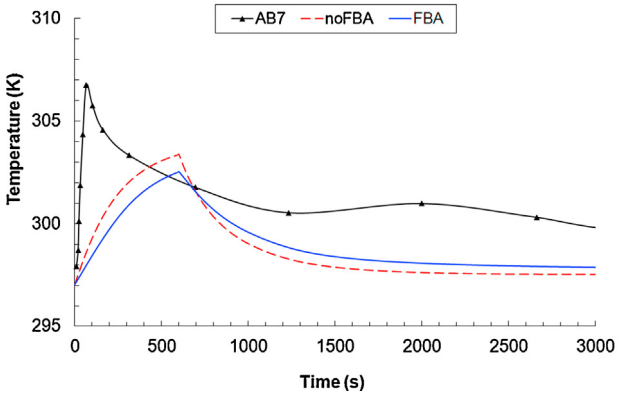

Fig. A.5. Atmosphere T – AB7 (MELCOR code).

presence of a columnar sodium fire during the first few seconds of the test.

A weakness of the FBA approximation is that the artificial surface area remains constant all over time. Actually, particles remain airborne for some time and gradually get removed from atmosphere by deposition mechanisms. Therefore, this approximation should result in an overestimate of gas and vessel wall temperatures during the aerosol deposition phase.

Appendix B. BE methodology

This appendix explores alternative parameter settings and shows the methodology developed to find out the most favourable scenario, what has been called best estimate (BE).

The "best estimate methodology" consists of several successive steps, as displayed in Fig. B.1. Next, it is illustrated for the MELCOR code – AB5 test.

B.1. Identification of uncertain parameters

There are several input parameters related to aerosol characterization and dynamics that might have an effect on aerosol behaviour. Some of those parameters affect particle–particle interactions: the agglomeration shape factor (γ), which enhances particles collision when they are not spherical; the sticking coefficient (STICK), which is the agglomeration probability of two colliding particles; or the turbulence dissipation rate (ε), which influences the inertial and shear turbulent agglomeration rate. Some other parameters affect the particle dynamics: the aerodynamic shape factors (χ), which slows down moving particles when they are not spherical; the slip coefficient (F_{slip}), which accounts for the momentum exchange between gas molecules and moving particles; or the ratio of gas-to-particle thermal conductivities (k_{gas}/k_p). And, finally, there are

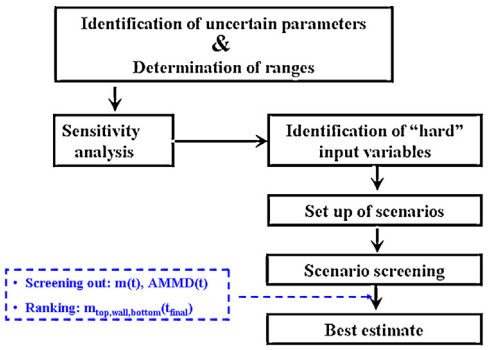

Fig. B.1. "Best estimate methodology" flow chart.

Table B.1
Aerosol coefficient ranges.

Aerosol coef.	BC	Range used
χ	1.0	1.0–5.0
γ	1.0	1.0–5.0
F_{slip}	1.257	1.14, 1.257
STICK	1.0	0.5, 1.0
ε (m^2/s^3)	0.001	0.001, 0.02
k_{gas}/k_p	0.05	0.06
c_t	2.25	2.18, 2.25
δ_{diff} (m)	1e−5	1e−5, 1e−3

others which affect specific aerosol removal processes: the thermal accommodation coefficient (c_t), which is the fraction of thermal energy transferred from a particle to the surface on which it is depositing; or the diffusion boundary layer thickness (δ_{diff}), which magnitude determines the concentration gradient driving diffusion. Through a literature survey (Allelein et al., 2009; Epstein and Ellison, 1988; Gauntt et al., 2005; Gieseke et al., 1977; Helton et al., 1986; Klein-Hessling and Schwinges, 1998; Lee et al., 1978; Loyalka, 1983; Murata et al., 1997; NEA-CSNI, 1979; Talbot et al., 1980; Williams et al., 1987) the ranges of interest of these parameters have been found (third column in Table B.1).

B.2. Identification of "hard" input variables

Among all these parameters, some stand out due to their significant influence, while others' effect is much less. The criterion set has been that final mass distribution (particularly, the amount of mass on the vessel lower head) is changed more than 10% when using the extreme values in the ranges. Three cases have been run for each individual parameter (the upper and lower bounds of the interval and an intermediate value). From these runs it has been stated that the "hard" parameters found have been: the shape factors (χ, γ) and the turbulence dissipation rate (ε).

B.3. Scenarios selection

Once the "hard input variables" were identified, a set of 15 cases have been run (Table B.2). Fig. B.2 compiles the results obtained in terms of airborne mass along with data.

In order to choose the most favourable scenario, two criteria are used, which are named according to their nature: "evolution-based", which relies on similarity between predictions and measurements of airborne mass (variations less than 20%) and

Table B.2
Aerosol scenario screening.

Case	χ	γ	ε (m^2/s^3)
1	1	1	0.02
2	2	2	0.001
3	2	2	0.02
4	2	2.5	0.02
5	2	2.5	0.001
6	1.75	2.5	0.001
7	1.75	2.75	0.001
8	2.5	2.5	0.001
9	2.25	2.25	0.001
10	2.5	2.5	0.02
11	2.25	2.5	0.001
12	3	3	0.001
13	4	4	0.001
14	5	5	0.001
BC*	1	1	0.001
RC**	1.5	2.25	0.001

* BC (base case): aerosol coefficients values used in codes by default.
** RC (reference case): aerosol coefficients values as estimated by Souto et al. (1994).

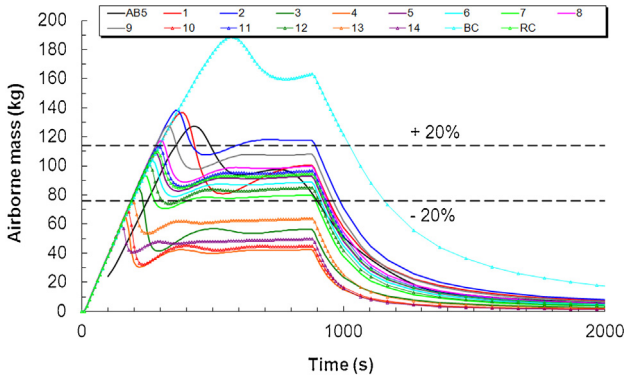

Fig. B.2. Airborne mass as a function of time.

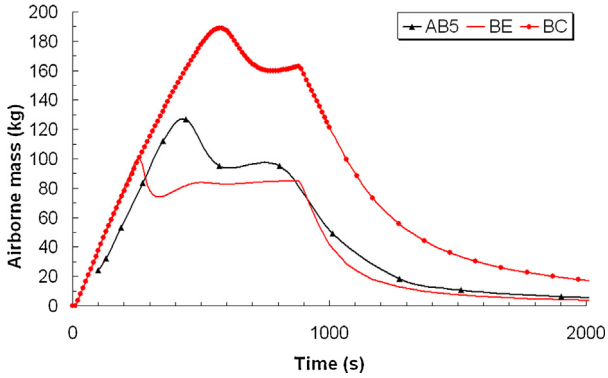

Fig. B.4. Airborne mass (BE vs. BC).

Aerodynamic Mass Median Diameter (AMMD); and "integral-based", which assess proximity to the final mass distribution observed. The former can be said to be qualitative since the cases selection is not based on any equation that yields a value on which to build a case ranking. Fig. B.3 shows the set of cases chosen for AB5 (MELCOR simulation).

The latter has been developed in a quantitative way and "proximity" to data has been assessed through,

$$\text{Proximity} = 1 - \text{Error} = 1 - \sum_{\text{i=location}} Y(\text{i}) \cdot \varepsilon_{\text{r}}(\text{i}) =$$

$$1 - Y_{\text{ceiling}} \cdot \frac{\left|\left(\varepsilon_{\text{ceiling}}^{\text{calculated}} - \varepsilon_{\text{ceiling}}^{\text{data}}\right)\right|}{\varepsilon_{\text{ceiling}}^{\text{data}}} + Y_{\text{wall}} \cdot \frac{\left|\left(\varepsilon_{\text{wall}}^{\text{calculated}} - \varepsilon_{\text{wall}}^{\text{data}}\right)\right|}{\varepsilon_{\text{wall}}^{\text{data}}}$$

$$+ Y_{\text{bottom}} \cdot \frac{\left|\left(\varepsilon_{\text{bottom}}^{\text{calculated}} - \varepsilon_{\text{bottom}}^{\text{data}}\right)\right|}{\varepsilon_{\text{bottom}}^{\text{data}}}$$

where $Y(\text{i})$ is the weighting factor of a "i" location according to its experimental contribution to the total mass deposited. In other words a deviation from data at the bottom affects much more than the same deviation at the ceiling.

Application of both criteria to the cases in Fig. B.3 results in what has been called the best estimate (BE). Fig. B.4 shows the BE together with the BC and data. As noted, the BE provides a much better agreement with experimental trends than BC. The new scenario shortens the time to reach the maximum and the steady state, bringing estimates much closer to data. In other words, the trade off between particle injection and removal is reached earlier and at noticeable lower values of airborne mass than those of the BC calculations. As the main depletion process is sedimentation, this trend means that non-spherical particles speeds up agglomeration so much that the resulting size compensates the slowdown effect that non-sphericity has on the settling velocity.

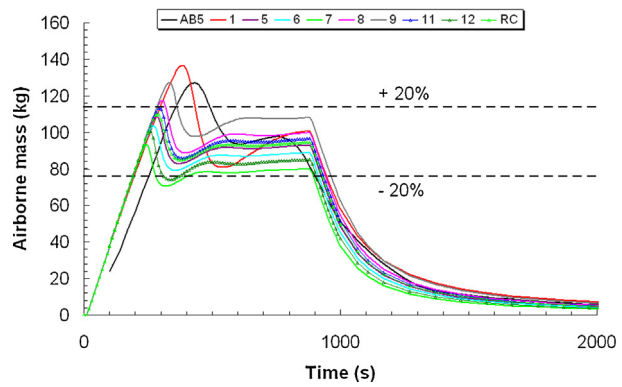

Fig. B.3. Airborne mass for the selected cases.

Table B.3
Aerosol coefficient values for the BE.

Test	Case (χ, γ, ε)		
	ASTEC	ECART	MELCOR
AB5	12 (3, 3, 0.001)	–(1.25, 2.75, f(v)*)	12 (3, 3, 0.001)
AB6	10 (2.5, 2.5, 0.02)	–(1.25, 2.75, f(v)*)	10 (2.5, 2.5, 0.02)
AB7	BC (1.0, 1.0, 0.001)	–(1.25, 2.25, f(v)*)	BC (1.0, 1.0, 0.001)

* This parameter is calculated as function of the velocity (ECART code).

Table B.3 shows the values resulting for the BE. As main observation, sodium based particles produced during a spray fire might be non-spherical; however, in the case of a pool fire (AB7), the results show that the aerosols generated might be spherical. The effect of high turbulence on the particle agglomeration in AB6 can be observed through the values obtained for the turbulence dissipation rate. These results highlight the relevance of setting suitable values for the aerosols coefficients, due to their impact on the results obtained.

References

Allelein, H.J., Auvinen, A., Ball, J., Güntay, S., Herranz, L.E., Hidaka, A., Jones, A., Kissane, M., Powers, D., Weber, G., 2009. State of the Art Report on Nuclear Aerosols. CSNI Report, NEA-CSNI/R(2009)5.

Clough, W.S., Garland, J.A., 1971. The behaviour in the atmosphere of the aerosol from a sodium fire. J. Nucl. Energy 25, 425–435.

Cooper, D.W., 1980. Prediction of the rates of chemical transformation of sodium fire aerosols. In: Proceedings of the CSNI Specialists Meeting on Nuclear Aerosols in Reactor Safety, NUREG/CR-1724, ORNL/NUREG/TM-404, CSNI-45, pp. 221–235.

Dunbar, I.H., Fermandjian, J., 1984. Comparison of Sodium Aerosol Codes. CEC Report EUR 9172.

Dunbar, I.H., 1985. Aerosol behaviour codes, development, intercomparison and application. In: Proceedings of the CSNI Specialist Meeting on Nuclear Aerosols in Reactor Safety, Karlsruhe, CSNI-95, pp. 471–485.

Epstein, M., Ellison, P.G., 1988. Correlations of the rate of removal of coagulating and depositing aerosols for application to nuclear reactor safety problems. Nucl. Eng. Des. 107, 327–344.

Fermandjian, J., 1985. Comparison of computer codes related to the sodium oxide aerosol behaviour in a containment building. In: Proceedings of the CSNI Specialist Meeting on Nuclear Aerosols in Reactor Safety, Karlsruhe, CSNI-95, pp. 486–497.

Fiorini, G.L., 2009. European commission-7th framework program. The collaborative project on European sodium fast reactor (CP ESFR). In: Proceedings of ICAPP '09, Tokyo, Japan, pp. 10–14.

Gauntt, R.O., Cash, J.E., Cole, R.K., Erickson, C.M., Humphries, L.L., Rodriguez, S.B., Young, M.F., 2005. MELCOR Computer Code Manuals. NUREG/CR-6119, SAND2005-5713.

Gelbard, F., 1982. MAEROS User Manual. NUREG/CR-1391 SAND80-0822.

Gieseke, J.A., Reed, L.D., Jordan, H., Lee, K.W., 1977. Characteristics of Agglomerates of Sodium Oxide Aerosol Particles. BMI-NUREG-1977.

Helton, J.C., Iman, R.L., Johnson, J.D., Leigh, C.D., 1986. Uncertainty and sensitivity analysis of a model for multicomponent aerosol dynamics. Nucl. Technol. 73, 322.

Herranz, L.E., Ball, J., Auvinen, A., Bottomley, D., Dehbi, A., Housiadas, C., Piluso, P., Layly, V., Parozzi, F., Reeks, M., 2010. Progress in understanding key aerosol issues. Prog. Nucl. Energy 52, 120–127.

Herranz, L.E., García, M., Kissane, M.P., 2012. In-containment source term in accident conditions in sodium-cooled fast reactors: data needs and model capabilities. Prog. Nucl. Energy 54, 138–149.

Hilliard, R.K., McCormack, J.D., Muhlestein, L.D., 1985. Results and Code Predictions for ABCOVE Aerosol Code Validation with Low Concentration NaOH and NaI aerosol – CSTF TEST AB7. HEDL-TME 85-1.

Humphreys Jr., J.R., 1958. Sodium-air reactions as they pertain to reactor safety and containment. Proceedings of Second Geneva Conference, 11., pp. 180.

Klein-Hessling, W., Schwinges, B., 1998. CPA Module: Program Reference Manual. Report ASTEC-V0/DOC/01-34.

Lee, K.W., Gieseke, J.A., Reed, L.D., 1978. Sensitivity Analysis of the HAARM-3 Code, NUREG/CR-0527 BMI-2008.

Lee, Y.B., Choi, S.K., 1997. A study on the development of advanced model to predict the sodium pool fire. J. Korean Nucl. Soc. 29, 240–250.

Loyalka, S.K., 1983. Mechanics of aerosols in nuclear reactor safety: a review. Prog. Nucl. Energy 12, 1–56.

Morewitz, H.A., 1979. Sodium spray fires. Nucl. Eng. Des. 55, 275–281.

Murata, K.K., Williams, D.C., Tills, J., Griffith, R.O., Gido, R.G., Tadios, E.L., Davis, F.J., Martinez, G.M., Washington, K.E., 1997. Code Manual for CONTAIN 2.0: A Computer Code for Nuclear Reactor Containment Analysis, NUREG/CR-6533.

NEA-CSNI, 1979. Nuclear aerosols and reactor safety. In: A State-of-the Art Report by a Group of Experts of the NEA Committee on the Safety of Nuclear Installations, Appendix A.

Newman, R.N., 1983. The ignition and burning behaviour of sodium metal in air. Prog. Nucl. Energy 12, 119–147.

Okano, Y., Yamaguchi, A., 2003. Theoretical adiabatic temperature and chemical composition of sodium combustion flame. Nucl. Technol. 144 (3), 388–399.

Parozzi, F., et al., 2011. ECART CODE User's Manual. RSE Technical Report, 2011.

Souto, F.J., Haskin, F.E., Kmetyk, L.N., 1994. MELCOR 1.8.2 Assessment: Aerosol Experiments ABCOVE AB5, AB6, AB7 and LACE LA2. SAND94-2166.

Subramani, A., Jayanti, S., 2008. Equilibrium considerations in aerosol formation during sodium combustion. Nucl. Eng. Des. 238, 2739–2745.

Talbot, L., Cheng, R.K., Schefer, R.W., Willis, D.R., 1980. Thermophoresis of particles in a heated boundary layer. J. Fluid Mech. 101, 737–758.

Williams, D.C., Bergeron, K.D., Rexroth, P.E., Tills, J.L., 1987. Integrated phenomenological analysis of containment response to severe core damage accidents. Prog. Nucl. Energy 19, 59–131.

Yamaguchi, A., Tajima, Y., 2006. A numerical study of radiation heat transfer in sodium pool combustion and response surface modelling of luminous flame emissivity. Nucl. Eng. Des. 236, 1179–1191.